

Themes and Variations in ER/SR Calcium Release Channels: Structure and Function

Calcium (Ca^{2+}) release from reticular stores is a vital regulatory signal in eukaryotes. Recent structural data on large NH_2 -terminal regions of IP_3Rs and RyRs and their tetrameric arrangement in the full-length context reveal striking mechanistic similarities in Ca^{2+} release channel function. A common ancestor found in unicellular genomes underscores the fundamentality of these elements to Ca^{2+} release channels.

Peter B. Stathopoulos,^{1*}
Min-duk Seo,^{2*} Masahiro Enomoto,^{1*}
Fernando J. Amador,^{1*}
Noboru Ishiyama,^{1*}
and Mitsuhiro Ikura¹

¹Ontario Cancer Institute and Department of Medical Biophysics, University of Toronto, Toronto, Ontario, Canada; and ²College of Pharmacy, Ajou University, Suwon, Korea
mikura@uhnres.utoronto.ca

*P. B. Stathopoulos, M. Seo, M. Enomoto, F. J. Amador, and N. Ishiyama contributed equally to this work.

The calcium (Ca^{2+}) ion is a universal messenger that controls a vast number of cellular processes such as the prolonged regulation of transcription, cell division, and apoptosis, as well as the more short-lived secretion and contraction (5, 6). The Ca^{2+} ion plays an indispensable role in contractile, neuronal as well as nonexcitable cells (4–6, 133, 136, 137). At rest, cells compartmentalize most intracellular Ca^{2+} ($[\text{Ca}^{2+}]_i$) in the sarco-/endoplasmic reticulum (SR/ER) stores. Upon stimulation, Ca^{2+} is released from the SR/ER into the intracellular space (i.e., cytosol); the spatial and temporal release and uptake of $[\text{Ca}^{2+}]_i$ is the driving force behind these myriad cellular processes in health and disease.

There are two types of Ca^{2+} handling macromolecules on the SR/ER membrane: first, Ca^{2+} release receptor-operated channels (ROCs) liberate internally stored Ca^{2+} into the cytoplasm; second, Ca^{2+} pumps replete the internal store of Ca^{2+} . The SR/ER Ca^{2+} ATPase (SERCA) pumps are a major family of SR/ER-residing Ca^{2+} pumps that have been the topic of review in the past (82, 131). The two major groups of Ca^{2+} release channels include the ubiquitously expressed inositol 1,4,5-trisphosphate receptors (IP_3Rs) and the ryanodine receptors (RyRs) found more exclusively in excitable cells. These ROCs belong to a voltage-independent class of Ca^{2+} channels; nonetheless, RyR function is intimately tied to voltage-operated channels (VOCs) in various cell types through excitation-contraction coupling and Ca^{2+} -induced Ca^{2+} release (CICR). Although RyR channels can be regulated by ryanodine binding (i.e., $\sim\text{nM}$ concentrations open the channel, whereas sub-mM concentrations inhibit the channel) (80), Ca^{2+} binding itself triggers RyR channel opening, and RyRs can propagate Ca^{2+} signals within a cell through responses to $[\text{Ca}^{2+}]_i$ (33, 34). Hence, excitation-contraction coupling within excitable cells can occur as L-type Ca^{2+} VOCs increase $[\text{Ca}^{2+}]_i$, thereby stimulating further Ca^{2+} release via RyRs .

Although Ca^{2+} binding is a potent agonist of RyR channel opening, higher levels actually induce channel closure. IP_3Rs absolutely require inositol 1,4,5-trisphosphate (IP_3) for activation; however, they also can be considered CICR channels similar to RyRs , since cytosolic Ca^{2+} has a comparable bell-shaped effect on the open probability of the Ca^{2+} channel pore (102). Extracellular agents can trigger $[\text{Ca}^{2+}]_i$ release from intracellular stores through activation of specific cell surface receptors and engagement of the signal transduction pathway, which involves activation of phospholipase C (PLC); furthermore, the phospholipase-dependent catalysis of phosphatidylinositol 1,4-bisphosphate liberates IP_3 , the diffuseable messenger that binds to and activates IP_3Rs .

Overall, CICR channels are interrelated by an ability to permeate Ca^{2+} , a functional sensitivity to local Ca^{2+} concentrations and by an organization on membranes that facilitates Ca^{2+} -mediated communication between like macromolecules (127). The IP_3Rs and RyRs share these CICR features as transmembrane ROCs with similar but distinct structural and functional characteristics. Architecturally, vertebrate IP_3Rs and RyRs are large proteins forming functional channels as symmetric tetramers. The ion-conducting region of IP_3Rs and RyRs share a high sequence homology. Furthermore, the commonalities between these ROCs spread beyond the pores, with conserved mannosyl-transferase, IP_3R , RyR (MIR), internal RyR and IP_3R homology (RIH), as well as RIH-associated domains before the transmembrane regions. MIR domains are a series of ~ 200 amino acid repeats near the NH_2 terminus, also found in yeast *o*-mannosyl-transferase that do not form discrete IP_3 -binding sites (72). RIH domains are also located near the NH_2 terminus, exhibiting sequence and structural homology to the IP_3 -binding core of IP_3Rs (97). Calcium release channels often contain RIH domains coupled with RIH-associated domains, an ~ 100 amino acid domain preceding the

pore-forming regions (72, 97). RyRs, which are composed of almost double the number of amino acids as IP₃Rs, diverge from IP₃Rs with the insertion of several NH₂-terminal and COOH-terminal pore-intervening SPRY (SP1a and RyR) domains. SPRY domains share low sequence identity and function as protein-interaction domains (121). The conserved architectural features found in IP₃Rs and RyRs suggest the presence of a common ancestor for these ROCs in lower order organisms.

The present review focuses on new structural insights on the NH₂-terminal regions of IP₃Rs and RyRs and the tetrameric arrangement of these regions exhibiting high structural homology in the full-length context. Additionally, we highlight genomic analyses identifying this class of ROCs in unicellular organisms and the implications of these data in understanding the molecular evolution of these fundamental receptors in nature.

Genomic Analyses and Domain Organization of IP₃Rs and RyRs

The *IP₃R* genes encode large proteins (~2,700 amino acids residues) that assemble into tetrameric functional channels. The *RyR* gene encodes an even larger subunit (~5,000 amino acid residues), also forming a tetrameric channel on the membrane. Three isoforms of IP₃Rs (IP₃R1, IP₃R2, and IP₃R3) and RyRs (RyR1, RyR2, and RyR3) have been identified in mammalian vertebrates (9, 26, 38, 52, 65, 73, 81, 91, 104, 118). In nonmammalian vertebrates such as birds and fish, two to three IP₃R isoforms and two RyR isoforms (RyR α and RyR β) are expressed (92, 120). In mammals, the three IP₃R isoforms are ubiquitously expressed and have distinct and overlapping distribution patterns; cells in the central nervous system predominantly or solely express IP₃R1, whereas most other cells express more than one type (14, 27, 28, 84, 89, 116, 124, 126, 132). The RyR1 isoform is primarily expressed in skeletal muscle (122, 141), whereas the predominant form of RyR in cardiac muscle is RyR2 (85, 91). RyR2 is also expressed at high levels in Purkinje cells of the cerebellum and the cerebral cortex (37, 62, 86, 115). RyR3 is expressed in hippocampal neurons, thalamus, Purkinje cells, corpus striatum (37, 42, 62), skeletal muscles (75, 90), and smooth muscle (39, 40, 43, 92).

Although RyRs can be activated by Ca²⁺ alone, IP₃Rs are classified as a dual-ligand gated channel whose opening is induced by IP₃ and Ca²⁺ (7, 35, 49, 50). Additionally, a diverse number of molecules are known as modulators of IP₃Rs and RyRs and are largely responsible for distinctions in function. IP₃R channel activity can be regulated by divalent cations, ATP, PKA, PKG, CaMKII, Akt,

CaM, CaBP1, ERp44, IRBIT, RACK1, 4.1N, Homer, TRPC, and Na⁺-K⁺-ATPase, to name a few (36, 127). Similarly, RyR function is modulated by molecules such as ryanodine, Mg²⁺, ATP, PKA, CaMKII, Ca_v1.1, CaM, calsequestrin, and FKBP12 (65).

Despite vast differences in protein size, vertebrate IP₃Rs and RyRs share a similar domain architecture (FIGURE 1A). Both receptors possess pore-forming transmembrane helices at the COOH terminus, contain critical NH₂-terminal cytosolic domains that regulate the channel helices, and have large cytoplasmic regulatory domains sandwiched between the NH₂ and COOH termini. Recently, the crystal structures of NH₂-terminal domains of rat IP₃R1 (*residues 1–604*) and rabbit RyR1 (*residues 1–559*) were revealed to be strikingly similar despite low sequence identity (111), the topic of detailed discussion below. These functional and structural similarities between vertebrate IP₃Rs and RyRs suggest a common ancestry between IP₃R and RyRs. In multicellular invertebrates, genes encoding IP₃R, *itr-1*, and RyR, *unc-68*, have been identified in *Caenorhabditis elegans* (3, 76, 107). Despite studies in past decades identifying G-protein-coupled receptors and IP₃-associated second messenger systems in unicellular eukaryotes (17, 22, 77), only recent genomic analyses have revealed the presence of putative IP₃Rs and RyRs in *Monosiga brevicollis*, *Salpingoeca rosetta*, and *Capsaspora owczarzewski*, the closest unicellular relatives of animals (15, 16). Putative IP₃R/RyR homologs have also recently been identified in pathogenic unicellular parasites including *Trypanosoma brucei*, *Trypanosoma cruzi*, *Leishmania major*, and *Leishmania infantum* (97).

The phylogenetic relationship of IP₃Rs and RyRs in unicellular and multicellular eukaryotes suggests that the divergence of IP₃Rs and RyRs occurred along with or shortly before the emergence of multicellular organisms, since the IP₃R/RyR homolog in *Trypanosoma* and *Leishmania* branched out before the IP₃Rs and RyRs (FIGURE 1B). Hence, these homologs are likely common ancestors to the eukaryotic Ca²⁺ release channels and may possess a rudimentary activation mechanism, the critical features of which are inherited by IP₃Rs and RyRs in multicellular animals. For example, the unicellular IP₃R and RyR homologs show a high degree of similarity (~40%) in the pore region responsible for ion conductance compared with mouse IP₃R1 (*residues 2,527–2,596*) and mouse RyR1 (*residues 4,874–4,942*), highlighting the pore region as a key structural feature in intracellular Ca²⁺ channel function. The IP₃R/RyR homologs in *Trypanosoma* and *Leishmania* are much shorter than RyRs found in multicellular animals, and evaluation of the genomes for the presence of an IP₃-binding domain (i.e., based on mouse IP₃R1 *residues 224–604*) confirms a

closer homology to IP₃Rs than RyRs, despite lacking many of the basic residues essential for high-affinity IP₃ binding in vertebrates (10). These data, taken together with the fact that only IP₃R (i.e., not RyR) has been identified in the unicellular *Paramecium* (61), suggest that RyRs appeared later in evolution. Future high-resolution structural work should provide further insight into the molecular evolution of this class of receptors. At present, detailed structural data exists only for the NH₂-terminal domains of the vertebrate IP₃R and RyRs; nonetheless, the data have provided a wealth of knowledge on the commonalities in mechanistic action between IP₃Rs and RyRs.

Atomic Resolution Structures of the NH₂-Terminal Domains of IP₃Rs and RyRs

The NH₂-terminal region of vertebrate IP₃Rs, which resides in the cytosol, contains two functional domains: the suppressor domain (SD; residues 1–223 of IP₃R1) and the IP₃-binding core (IBC; residues 224–604 of IP₃R1). The first high-resolution structure determined by X-ray crystallography was the IBC of IP₃R1 (PDB code 1N4K) (10). The structure of the IBC in complex with IP₃ contains two structurally distinct domains: the β-domain

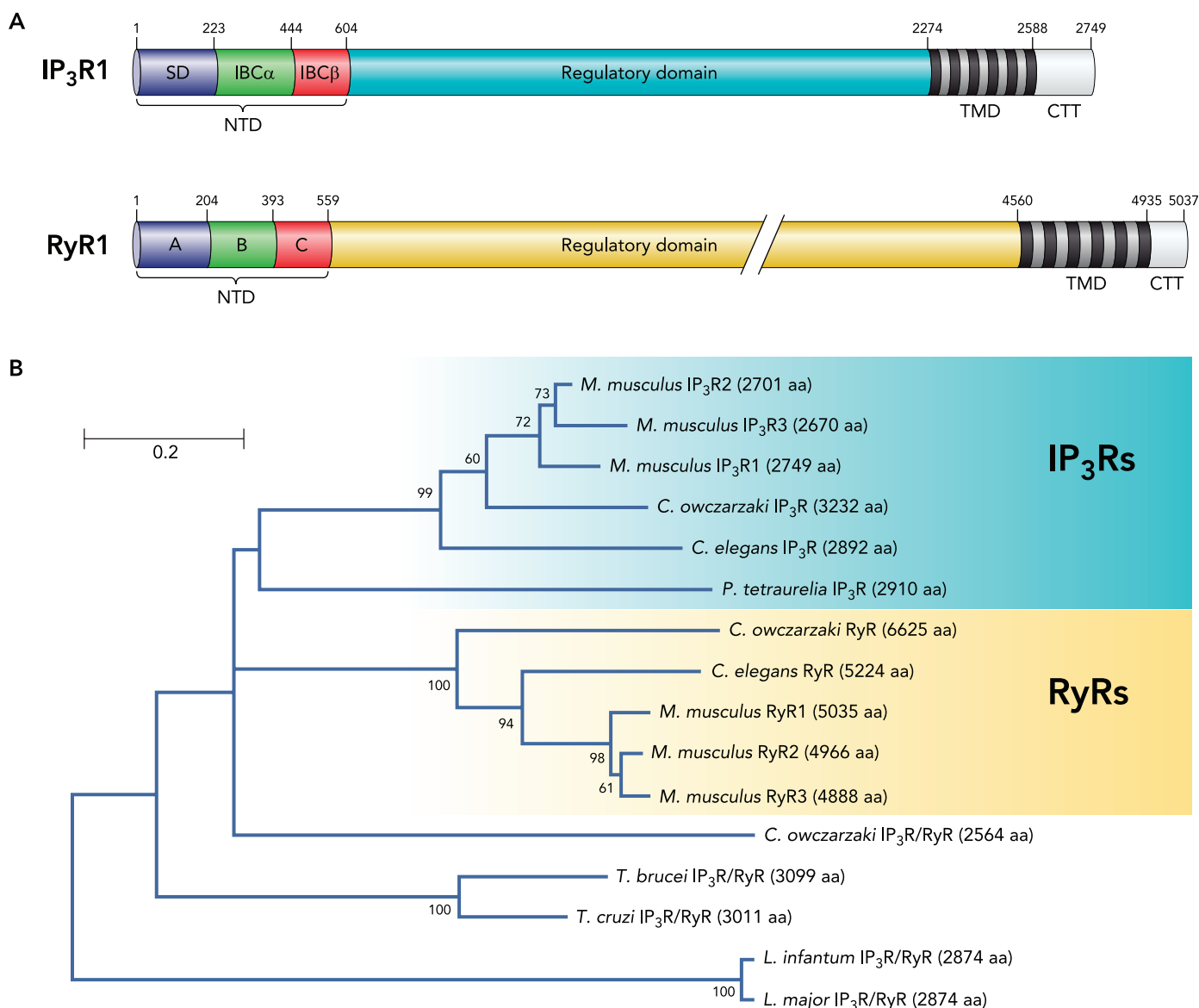


FIGURE 1. Domain organization and genomic analyses of IP₃Rs and RyRs

A: domain architecture for IP₃R and RyR. The numbers on top of the domain diagram represent the amino acid residues of rat IP₃R1 and rabbit RyR1. NTD, NH₂-terminal domain; SD, suppressor domain; IBC, IP₃-binding domain; TMD, transmembrane domain; CTT, COOH-terminal tail. B: maximum likelihood phylogenetic tree showing the relationship between IP₃R and RyR homologs in uni- and multicellular eukaryotes. The blue and yellow shades separate the sequences of IP₃Rs and RyRs. Bootstrap values of >50 are shown at the nodes. The scale bar represents amino acid substitutions per site. Multiple sequence alignments were made with MAFFT using default parameters (58). After using Gblocks 0.91b (19) at low stringency to remove regions of low confidence and gaps, maximum likelihood analysis was carried out using MEGA 5.0 using default parameters with the WAG substitution model (123) (100 boot-strapped data sets).

(IBC- β) and α -domain (IBC- α). The IBC- β (residues 224–436 of IP₃R1) adopts a β -trefoil fold comprising 12 β -strands and two single turn helices, whereas the IBC- α (residues 437–604 of IP₃R1) adopts an armadillo repeat fold consisting of 8 α -helices (FIGURE 2A). The IBC forms an L-shaped structure with the two domains oriented approximately perpendicular to each other, and the basic amino acids located in the cleft formed by both domains comprising the IP₃ binding site. The crystal

structures of the SD have been determined for IP₃R1 (residues 1–223 of IP₃R1, PDB code 1XZZ) (11) and IP₃R3 (residues 1–224 of IP₃R3, PDB code 3JRR) (21); moreover, the two structures are nearly identical (FIGURE 2B). The SD folds into a hammer-like structure with a 12- β -stranded “head” domain and a helix-turn-helix “arm” domain. Furthermore, the head domain of the SD adopts a similar β -trefoil fold found in the IBC; however, the molecular surfaces of specific

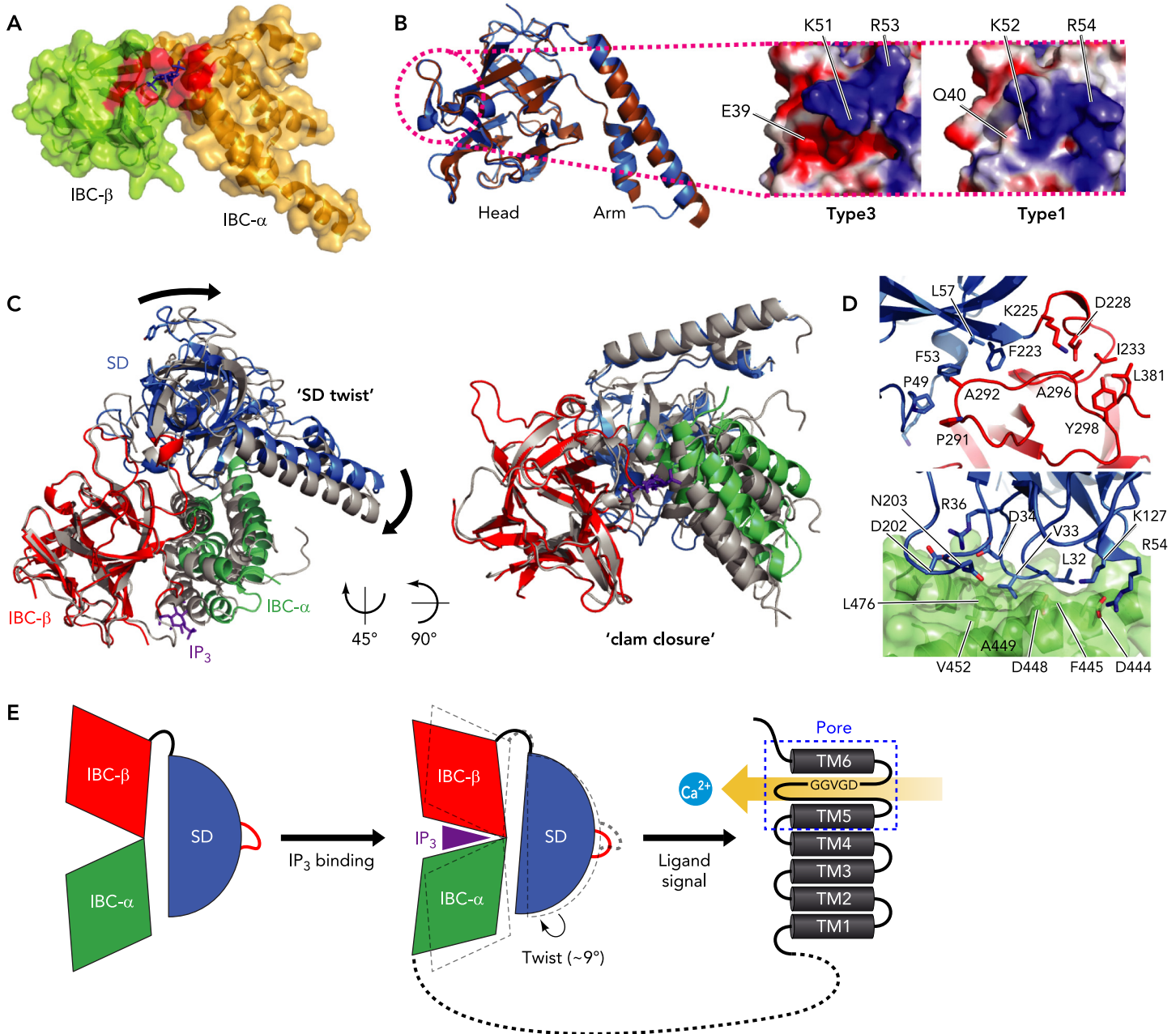


FIGURE 2. Structural features of the IP₃R-NT region

A: structure of the IBC in complex with IP₃ at 2.2-Å resolution. Ribbon and surface representations of the IBC- β (light green) and IBC- α (orange) are shown, and the IP₃-coordinating residues are colored red. B: superimposed structures of the IP₃R1-SD (blue) and IP₃R3-SD (brown). The acidic pocket in IP₃R3-SD and the equivalent region in IP₃R1-SD are highlighted (magenta circle) and represented by electrostatic surface. C: superimposed apo-NT (SD, blue; IBC- β , red; IBC- α , light green) and IP₃-bound NT (gray) structures. The structures were aligned by overlaying the IBC- β . D: the two interfaces between the SD and IBC (colored as in C) domains. The β -interface (top) and α -interface (bottom) are shown. E: a model depicting the IP₃-evoked conformational changes and the coupling between SD and channel gating. The critical loop (including Tyr167 residue) for channel gating is colored red. The IP₃ molecule and transmembrane domains (TMD) are shown as a violet triangle and gray cylinders, respectively.

regions are considerably different between SDs from *type 1* (IP₃R1-SD) and *type 3* (IP₃R3-SD), and this may contribute to isoform-specific IP₃ binding affinity (51). Specifically, the IP₃R3-SD contains a small acidic pocket centered by the negatively charged Glu39 that is replaced by Gln40 in IP₃R1-SD; moreover, the side-chain orientation of Arg53 near the pocket in IP₃R3-SD is retracted compared with the orientation of the corresponding residue (Arg54) in IP₃R1-SD, which collapses the pocket (FIGURE 2B). It is noteworthy that subtype-specific IP₃ binding equilibrium dissociation constants (K_d) have been estimated in the range of 10⁻⁷, 10⁻⁸, and 10⁻⁶ M for *type 1*, *2*, and *3* IP₃R, respectively (51, 52). Furthermore, modifications to the SD, such as posttranslational phosphorylation and heteromeric protein interactions (e.g., with calmodulin, CaBP1, and RACK1), could potentially influence IP₃ binding affinity. Functionally, different sensitivities to IP₃ binding, through isoform-specific structural differences as described for IP₃R1 and IP₃R3, posttranslational modifications, or heteromeric protein-interactions, play a role in shaping the spatial and temporal Ca²⁺ release responses that drive specific cellular processes. Consistent with this notion, dynamically changing IP₃ sensitivity has been reported during Ca²⁺ oscillations in live cells (78).

The isolated IBC is the minimal domain required for IP₃ binding and shows a very high affinity for IP₃ in vitro ($K_d \sim 2.3$ nM). Remarkably, the affinity of the entire NH₂-terminal region (NT; *residues 1–604* of IP₃R1) is reduced by more than one order of magnitude ($K_d \sim 45$ nM), implying that the SD inhibits (or “suppresses”) the IP₃ binding (139). Not only is the SD required for suppression of IP₃ binding, but it is also needed for IP₃-induced allosteric channel gating. A single Tyr167Ala mutation in the SD attenuates IP₃-evoked Ca²⁺ release (138). Tyr167 is located on the exposed loop in the head domain of SD and oriented on the opposite face of the SD/IBC interfaces. Although the exact allosteric mechanism of the functional coupling between the SD and channel domain remains elusive, the critical loop in the SD that includes Tyr167 plays an important role in linking IP₃ binding to channel gating.

Recently, four atomic-resolution NT structures of IP₃R1 have been determined. Lin and colleagues solved two NT structures of rat IP₃R1 at 3.8-Å resolution; moreover, they were able to derive one structure in an IP₃-free state (i.e., apo) and a second structure in an IP₃-bound state (i.e., holo) from a single crystal grown in the presence of IP₃ (PDB code 3T8S) (66). Subsequently, the NT structures of rat IP₃R1 at higher resolution were separately determined from crystals grown in the absence (3.0 Å, PDB code 3UJ4) and presence

(3.6 Å, PDB code 3UJ0) of IP₃, respectively (111) (FIGURE 2C). The individual structures of the three domains comprising NT of IP₃R1 (i.e., SD, IBC-β, and IBC-α) are remarkably similar to the separately determined SD (PDB code 1XZZ) (11) and IBC (PDB code 1N4K) (10). Nonetheless, these NT structures represent a significant advancement in the understanding of IP₃R function by revealing the arrangement of the SD and IBC domains with respect to one another and providing important clues on the bases for tetrameric channel formation. The three domains in NT structure form a triangular structure, and the SD is located on the opposite face of the IP₃-binding site, suggesting that the SD suppresses the IP₃ binding by an allosteric mechanism (FIGURE 2C). The SD interacts with both the IBC-β and IBC-α, respectively, and forms two interfaces (i.e., β-interface and α-interface). The short β-interface consists predominantly of hydrophobic interactions between Pro49, Phe53, and Phe223 from the SD, and Pro291 and Ala292 from the IBC-β, and is supported by a salt bridge between Lys225 and Asp228 (FIGURE 2D, TOP). The longer α-interface is stabilized by hydrophobic interactions between Val33 in the SD and a pocket formed by nonpolar Val452, Phe445, Ala449, and Leu476 within IBC-α. Electrostatic interactions between Arg54 and Lys127 from the SD and Asp444 from IBC-α are also involved in forming the α-interface (FIGURE 2D, BOTTOM) (111). The functional importance of residues associated with the α-interface is demonstrated by the Val33Lys mutation, which almost completely abrogates the effects of the SD on IP₃ binding and attenuates the maximal open probability of the full-length channel (11, 105).

The most marked conformational change caused by IP₃ binding is the significant decrease in the domain orientation angle between IBC-β and IBC-α (FIGURE 2, C AND E). This ligand binding-induced structural change in IBC occurs with the hinge region set between IBC-β and IBC-α as a pivot point, resulting in a narrowing of the IP₃-binding cleft. Although the interdomain distance between SD and IBC-β at the β-interface slightly increases, the hydrophobic and electrostatic interactions forming the α-interface are retained after IP₃ binding; consequently, the SD rotates toward the IBC by ~9°, and twisting occurs approximately perpendicular to the closure of IBC. Ultimately, this subdomain reorientation within NT causes the movement of the exposed loop in the SD, including Tyr167 (FIGURE 2E).

The first X-ray studies on RyRs elucidated structures of the distal NH₂-terminal region (*residues 1–205*, domain A) for RyR1 (PDB code 3HSM) (1) and RyR2 (PDB code 3IM5) (69), demonstrating that domain A folds into a β-trefoil core consisting

of 12 β -strands and a single α -helix. Inheritable mutations in RyR1 and RyR2 have been linked with muscle contraction diseases including malignant hypothermia (MH) (12, 13, 18, 29, 31, 47, 57, 60, 64, 88, 93–95, 103, 106, 134), central core disease (CCD) (2, 30, 54–56, 98, 100, 101, 114, 140), catecholaminergic polymorphic ventricular tachycardia (CPVT) (25, 32, 41, 45, 46, 48, 59, 63, 67, 74, 87, 96, 128, 130, 135), and arrhythmogenic right ventricular dysplasia (ARVD) (23, 64, 83). These initial structures showed that a high frequency of disease-associated mutations for RyR1 (MH and CCD) and RyR2 (CPVT and ARVD) cluster in and around a loop connecting β 8 and β 9 [the hot spot (HS) loop] (1, 69). X-ray crystallography and nuclear magnetic resonance (NMR) experiments do not show any significant structural differences between the mutants and wild-type proteins, and biophysical analyses suggest no significant changes in stability (1, 69), unlike numerous other protein conformational disorders. Therefore, RyR mutations may perturb quaternary RyR interactions involved in tetrameric channel formation or interactions with modulatory proteins (119, 125).

More recent X-ray crystallography has revealed the structure of the first 559 residues of RyR1 (PDB code 2XOA), providing new insights into the effect of disease-associated mutations on RyR structure and function (129). This larger NH_2 -terminal construct encompasses three domains (i.e., A, B, and C). Although both domains A and B are comprised of β -trefoil cores (1, 69), domain C folds into a five-helix bundle (129). The domains interact with each other primarily via hydrophilic interactions, and 56 different disease-associated mutations from RyR1 and RyR2 can be mapped onto this larger structure (FIGURE 3A) (129). Most of these mutations are found at the intra-molecular interfaces between the three domains or inter-molecular contacts with neighboring ABC subunits in the tetrameric channel, as modeled by cryo-EM docking studies (see below). Interestingly, 19 of the 56 mutations (~33%) are modeled at the interface between domain A and B on different subunits (129). The HS loop in domain A (1, 69) and two flexible loops from domain B are important components of this inter-subunit interface (129). A second interface concentrated with mutations lies between domains A and C of the same subunit. This A–C intra-molecular interface is stabilized by two salt bridges: Arg45 from domain A interacts with Asp447 in domain C, whereas Asp61 and Glu40 from domain A form ionic bonds with Arg402 in domain C (FIGURE 3B) (129). Gel filtration and thermal melt experiments on the disease-associated Arg402Gly mutation show only minimal perturbations to the overall fold and stability of the structure (129). Lastly, several point mutations are

concentrated at the interface between domain A and electron-dense columns that extend toward the transmembrane domains (129). In addition to point substitutions within ABC, deletion of *exon 3* encoding a portion of domain A in RyR2 was linked to CPVT and other heart abnormalities in 16 members from two separate families (8, 79). Remarkably, the structural integrity of RyR2-A is rescued via the insertion of a flexible loop into the β -trefoil domain affected by the deletion resulting in enhanced thermal stability (68). Hence, CPVT is likely manifested by a disruption of interfaces with other domains for individuals carrying this *exon 3* deletion (68). The distribution of mutations on inter- and intra-molecular interfaces suggests that gating of the channel is allosterically coupled to the movement of individual domains relative to each other and on different subunits.

The three well folded and isolated domains of $\text{IP}_3\text{R1-NT}$ (SD, IBC- β , and IBC- α) can be superimposed on the corresponding domains of RyR1-ABC (A, B, and C) with a relatively low root mean square deviation in the backbone atoms (i.e., <3 Å). Furthermore, the relative orientation of the three domains is nearly identical when the full NT and ABC structures of $\text{IP}_3\text{R1}$ and RyR1 are superimposed (FIGURE 3B). The NT and ABC sequence identity and similarity are low (17% and 37%, respectively); however, the sequence and structure of the functionally important loop regions in the two receptors are conserved. In particular, the backbone and side-chain conformation of the critical loop in SD that is essential for channel gating of IP_3Rs is structurally homologous to the HS loop of RyR (FIGURE 3B, red box). The structural conservation between IP_3R and RyR is also readily apparent at the interfaces; the bidentate salt bridges stabilizing the α -interface of $\text{IP}_3\text{R1}$ (Arg54/Lys127 and Asp444) are preserved in the A–C interface of RyR1 (Glu40/Asp61 and Arg402), although with a reversal of charges (FIGURE 3B, black boxes). RyR1 exhibits a salt bridge at the A–C interface (Arg45 and Asp447) where mutational disruption results in disease and is not conserved in the α -interface of $\text{IP}_3\text{R1}$. The exceptionally high structural conservation observed for the cytosolic NH_2 -terminal regions of $\text{IP}_3\text{R1}$ and RyR1 extends to the quaternary arrangement of these domains on the membrane, and recent electron microscopy work has provided further insight into the structure-function relationships of this class of ROCs.

Cryo-Electron Microscopy of Tetrameric IP_3Rs and RyRs

Several groups have successfully employed cryo-electron microscopy (EM) to determine the quaternary arrangements of these proteins at nanometer

resolution (70, 71, 108). The IP₃R forms a ~1.2 MDa homotetrameric ion channel, and previous studies have suggested that multiple ligand-bound conformations exist in both open and closed states (20, 117). The inherent structural heterogeneity of the full-length IP₃R is underscored by the previous EM studies yielding inconsistent models determined at nominal resolution of 15–34 Å (24, 43, 44, 53, 110, 112). Recently, Ludtke et al. determined the cryo-EM structure of IP₃R1 isolated from the rat cerebellum at 9.5-Å resolution [EM Data Bank (EMDB) code 5278] by achieving higher image contrast through improved sample preparation (71). The tetrameric structure of IP₃R1 revealed a mushroom-shaped overall architecture with a fourfold symmetry axis along a central plug (FIGURE 4A). The cytoplasmic region is located above the transmembrane region with several large openings or “windows” between two regions (FIGURE 4B). The well defined transmembrane region shows that IP₃R1 contains many features of the ion-conduction pore assembly of K⁺ channels (FIGURE 4C) (71). In contrast, the cytoplasmic region consists of a relatively rigid exterior surface with a more structurally variable and flexible interior, possibly due to multiple conformations of IP₃R1 in the closed state.

The assembled RyR is the largest known membrane protein to date and forms a ~2.2 MDa tetramer (1). The cryo-EM structure of RyR1 isolated from the rabbit skeletal muscle was first revealed in its closed state at 2.4-nm resolution (99, 113) and further refined to ~10-Å resolution (EMDB codes 1275 and 5014) (70, 109). The tetrameric structure of RyR1 has an enormous cytoplasmic region that rests on top of a smaller transmembrane region with a fourfold symmetry axis along the ion conduction pore (FIGURE 4, D AND E). Although the cytoplasmic region of RyR1 does not contain a central plug or the perforations found in the IP₃R1 structure, the channel region resembles the ion-conduction pores of K⁺ channels (FIGURE 4F), as observed for IP₃R1. Furthermore, Samsó et al. used EGTA or an agonist, PCB 95, to selectively characterize the open and closed states of RyR1 bound to FKBP12 (EMDB codes 1607 and 1606, respectively) (108), revealing that a change in channel pore size is accompanied by the twisting movement of the transmembrane region as well as considerable conformational changes throughout the entire cytoplasmic region.

Together with the high-resolution crystal structures of the NH₂-terminal fragments (66, 111, 129), comparison of the cryo-EM structures of full-length IP₃R and RyR has revealed the architectural and functional similarities shared between these ROCs. Docking the crystal structures of IP₃R1-NT and RyR1-ABC into their full-length structures

shows that their NH₂ termini are located near the top of the cytoplasmic regions (FIGURE 4, B AND E). The IP₃R1 and RyR1 NH₂-terminal segments form remarkably homologous tetrameric rings around the fourfold symmetry axis, with the disease-associated HS loop of RyR1 (*residues 152–167*) and the equivalent loop of IP₃R1 (*residues 165–180*) involved in intersubunit interactions (FIGURE 4, A AND D). Hence, these observations indicate that the NH₂-terminal regions of RyRs and IP₃R1 play a critical role in the allosteric modulation of ion channel conductance through a modification of quaternary arrangements.

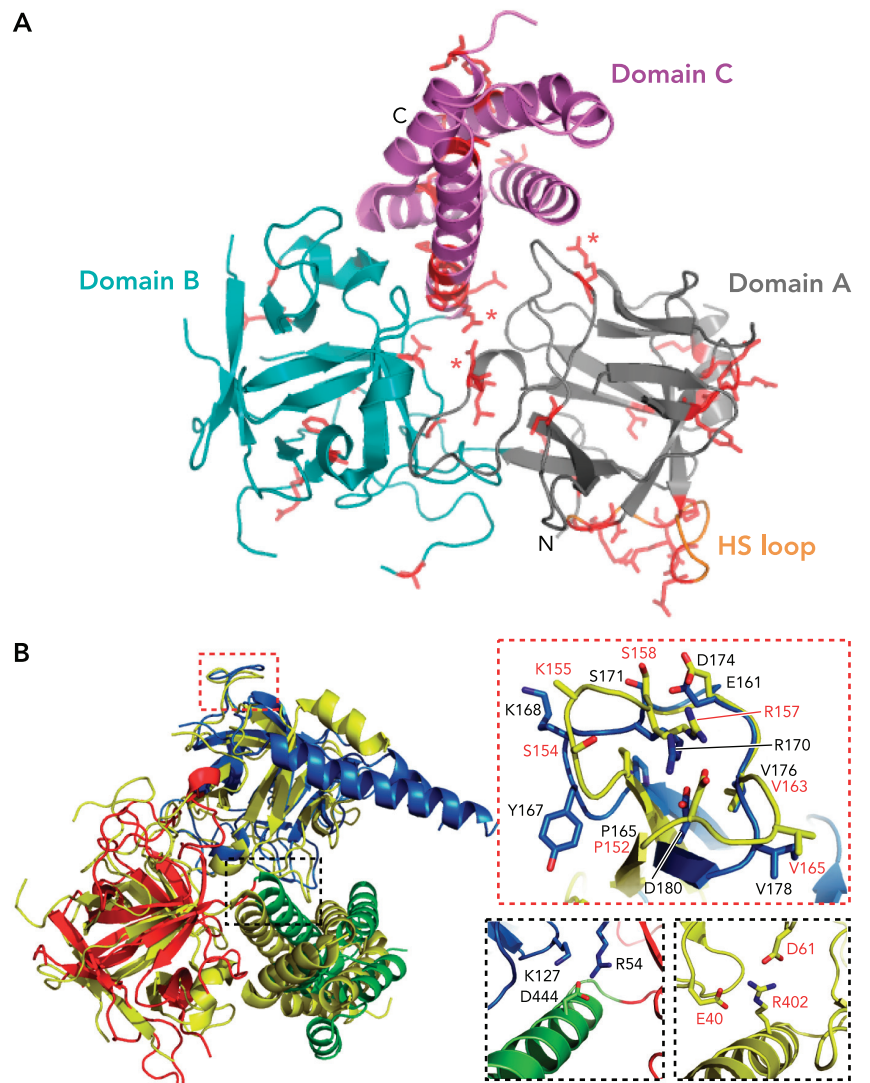


FIGURE 3. Disease-mutation localization and structural homology between RyR-ABC and IP₃R-NT

A: the structure of the ABC domain from RyR1 at 2.5-Å resolution. Domains A, B, and C are shown with disease-associated mutations highlighted in red. The HS loop is shown in orange, whereas mutations critical for salt-bridge formation are marked with asterisks. **B:** comparison of the NH₂-terminal structures of apo-IP₃R1 and RyR1 (yellow). The structures were aligned by overlaying IBC-β and domain B. The critical gating loop in IP₃R1 and the HS loop in RyR1 are highlighted with a red rectangle, and the conserved residues are represented as sticks in at *top right* (IP₃R1, black lettering; RyR1, red lettering). The α-interface of IP₃R1 and the corresponding interface in RyR1 are boxed with a black rectangle, and the preserved salt bridges are depicted in at *bottom right*.

Concluding Remarks

In multicellular eukaryotes, the universality of Ca^{2+} signaling has evolved with the versatility of the Ca^{2+} signaling toolkit in which IP_3R and RyR

are pivotal players (6). The conservation of these Ca^{2+} channels from unicellular eukaryotes to humans suggests that Ca^{2+} release from intracellular storage organelles through Ca^{2+} channels is a defining characteristic among eukaryotes. Structural

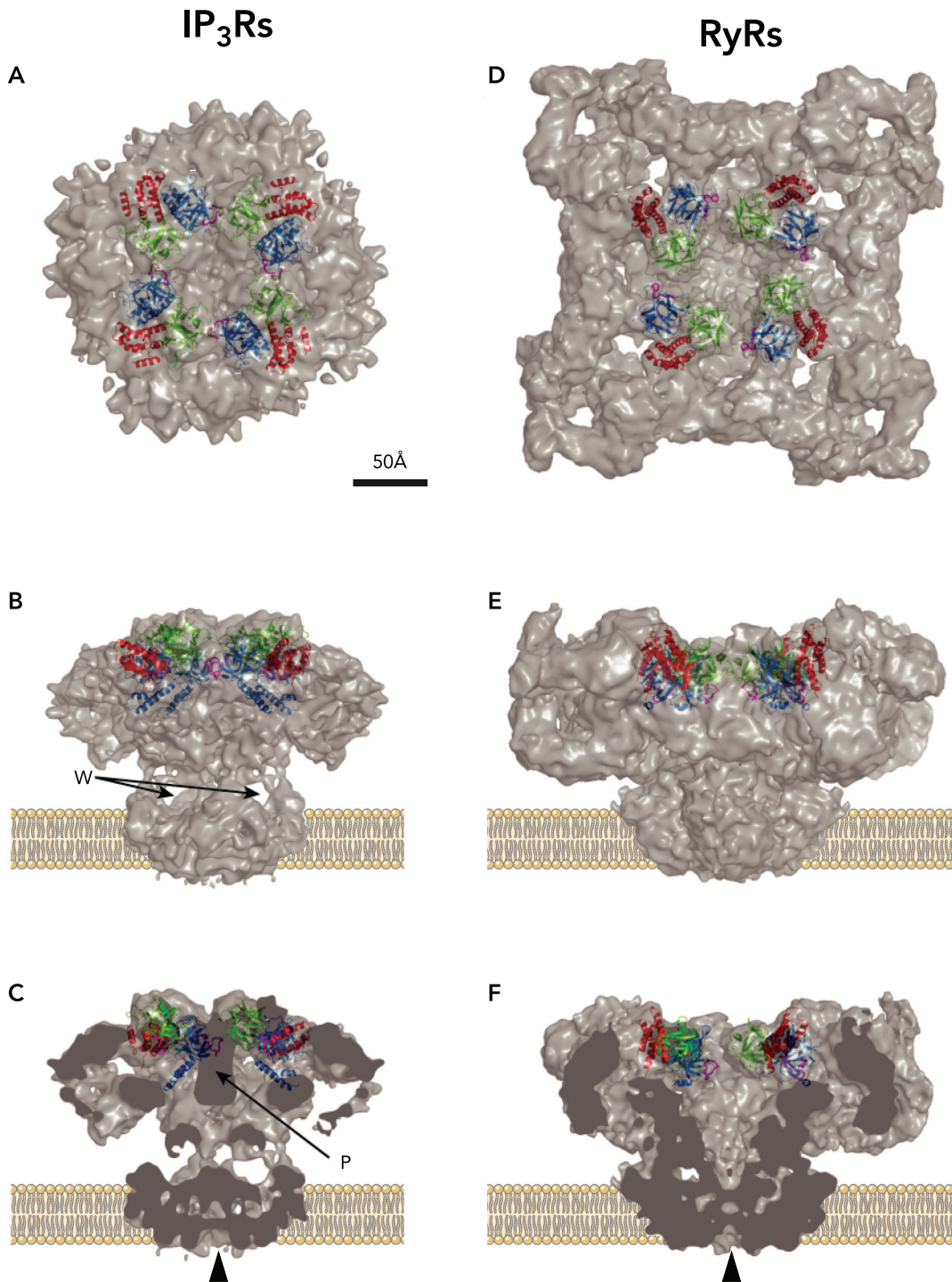


FIGURE 4. Structures of IP_3R and RyR tetramers

Cryo-EM structures of IP_3R (A–C) (EMDB code 5278) and RyR1 (D–F) (EMDB code 1275) in the closed state are shown from top (A and D) and side (B, C, E, F) views. Docked crystal structures of the NH_2 -terminal segments of IP_3R1 (PDB code 3UJ0) and RyR1 (PDB code 2XOA) are shown as ribbon representation with SD and A domains in blue, IBC- β and B domains in green, and IBC- α and C domains in red. The HS loops in RyR1-A and IP_3R1 -SD are indicated by magenta loops. In C and E, cryo-EM structures are sliced through the fourfold symmetry axis with the cutting plane in dark gray. The luminal side of the ion conduction pore is indicated by arrowheads. The central plug (P) and windows (W) of IP_3R are shown by arrows. The membrane bilayer is depicted as dotted lines. The scale bar applies to all panels in both dimensions.

and genomic analyses have highlighted the critical features of these IP₃R and RyRs, which include the ~600 structurally conserved distal NH₂-terminal residues, TMD pore-forming region, and quaternary assembly of these proteins. Despite the vast differences in molecular size between these ROCs, the fundamental nature of these elements to Ca²⁺ release channel function is corroborated by the evolutionary preservation of these characteristics from low- to high-order eukaryotic Ca²⁺ channels. Additionally, direct evidence for the importance of these elements is shown by experiments that exchange the SD of IP₃R1 with domain A of RyR1; these RyR1A-IP₃R1 chimeras maintain the ability to assemble into a tetrameric channel with similar IP₃ sensitivity and magnitude of Ca²⁺ release from ER stores as wild-type IP₃R1 in live cells (111). Furthermore, replacing the residues downstream of IP₃R1 TMD1 with the aligned TMDs from RyR1 produces a chimera capable of releasing ER Ca²⁺ in response to IP₃ binding with a channel pore that can be blocked by ryanodine, as per wild-type RyRs (111). Taken together, these data indicate a co-evolution of RyRs and IP₃R in eukaryotes and a functional interchangeability of key structural domains between these ROCs.

Marked advances in understanding the relationship between the structure and function of Ca²⁺ release ROCs have been made in the past decade highlighting the basis for signal transduction initiation by the NH₂-terminal IP₃R region along with a remarkable conservation in the overall structural architecture in the corresponding region of RyR, despite an absence of the IP₃ ligand binding property. Furthermore, reconstructed images of the tetrameric molecular arrangement of both receptors reveal a striking similarity in channel height in the membrane-anchored conformation despite the approximately twofold difference in polypeptide chain length. These important discoveries have brought new questions regarding the signaling and regulatory mechanisms of these Ca²⁺ ROCs to the forefront. First, how does Ca²⁺ binding regulate both IP₃R and RyR function in a bell-shaped manner? Second, how is IP₃R and RyR function distinctly modulated by the host of cellular signals such as phosphorylation, ATP binding, and smaller proteins (i.e., CaBP1), to name a few? Third, what are the structures of the channel pores and how do they change in response to these various cellular stimuli? Future structural and functional studies of IP₃R/RyR homologs in lower eukaryotes are also needed to enhance our understanding of the evolutionary significance of these Ca²⁺ toolkit components and to fully appreciate the rudimentary mechanisms of channel activation and modulation. ■

This work was supported by the Heart and Stroke Foundation of Canada (to M. Ikura) and the Canadian Institutes of Health Research (to M. Ikura and M.-D. Seo).

No conflicts of interest, financial or otherwise, are declared by the author(s).

Author contributions: P.B.S., M.-D.S., M.E., F.J.A., and N.I. prepared figures; P.B.S., M.-D.S., M.E., F.J.A., and N.I. drafted manuscript; P.B.S. and M.I. edited and revised manuscript; M.I. approved final version of manuscript.

References

- Amador FJ, Liu S, Ishiyama N, Plevin MJ, Wilson A, MacLennan DH, Ikura M. Crystal structure of type I ryanodine receptor amino-terminal beta-trefoil domain reveals a disease-associated mutation "hot spot" loop. *Proc Natl Acad Sci USA* 106: 11040–11044, 2009.
- Avila G, Dirksen RT. Functional effects of central core disease mutations in the cytoplasmic region of the skeletal muscle ryanodine receptor. *J Gen Physiol* 118: 277–290, 2001.
- Baylis H. Inositol 1,4,5-trisphosphate receptors are strongly expressed in the nervous system, pharynx, intestine, gonad and excretory cell of *Caenorhabditis elegans* and are encoded by a single gene (*itr-1*). *J Mol Biol* 294: 467–476, 1999.
- Berridge MJ. *Cell Signalling Biology*. London: Portland Press, 2009.
- Berridge MJ, Bootman MD, Roderick HL. Calcium signalling: dynamics, homeostasis and remodelling. *Nat Rev Mol Cell Biol* 4: 517–529, 2003.
- Berridge MJ, Lipp P, Bootman MD. The versatility and universality of calcium signalling. *Nat Rev Mol Cell Biol* 1: 11–21, 2000.
- Bezprozvanny I, Watras J, Ehrlich BE. Bell-shaped calcium-response curves of Ins(1,4,5)P₃- and calcium-gated channels from endoplasmic reticulum of cerebellum. *Nature* 351: 751–754, 1991.
- Bhuiyan ZA, van den Berg MP, van Tintelen JP, Bink-Boelkens MT, Wiesfeld AC, Alders M, Postma AV, van Langen I, Mannens MM, Wilde AA. Expanding spectrum of human RYR2-related disease: new electrocardiographic, structural, and genetic features. *Circulation* 116: 1569–1576, 2007.
- Blondel O, Takeda J, Janssen H, Seino S, Bell GI. Sequence and functional characterization of a third inositol trisphosphate receptor subtype, IP3R-3, expressed in pancreatic islets, kidney, gastrointestinal tract, and other tissues. *J Biol Chem* 268: 11356–11363, 1993.
- Bosanac I, Alattia JR, Mal TK, Chan J, Talarico S, Tong FK, Tong KI, Yoshikawa F, Furuichi T, Iwai M, Michikawa T, Mikoshiba K, Ikura M. Structure of the inositol 1,4,5-trisphosphate receptor binding core in complex with its ligand. *Nature* 420: 696–700, 2002.
- Bosanac I, Yamazaki H, Matsu-Ura T, Michikawa T, Mikoshiba K, Ikura M. Crystal structure of the ligand binding suppressor domain of type 1 inositol 1,4,5-trisphosphate receptor. *Mol Cell* 17: 193–203, 2005.
- Bouchama A, Knochel JP. Heat stroke. *N Engl J Med* 346: 1978–1988, 2002.
- Brandom BW, Larach MG, Chen MS, Young MC. Complications associated with the administration of dantrolene 1987 to 2006: a report from the North American Malignant Hyperthermia Registry of the Malignant Hyperthermia Association of the United States. *Anesth Analg* 112: 1115–1123, 2011.
- Bush KT, Stuart RO, Li SH, Moura LA, Sharp AH, Ross CA, Nigam SK. Epithelial inositol 1,4,5-trisphosphate receptors. Multiplicity of localization, solubility, and isoforms. *J Biol Chem* 269: 23694–23699, 1994.
- Cai X. Unicellular Ca²⁺ signaling "toolkit" at the origin of metazoa. *Mol Biol Evol* 25: 1357–1361, 2008.
- Cai X, Clapham DE. Ancestral Ca²⁺ signaling machinery in early animal and fungal evolution. *Mol Biol Evol* 29: 91–100, 2011.
- Calvert CM, Sanders D. Inositol trisphosphate-dependent and -independent Ca²⁺ mobilization pathways at the vacuolar membrane of *Candida albicans*. *J Biol Chem* 270: 7272–7280, 1995.

18. Capacchione JF, Muldoon SM. The relationship between exertional heat illness, exertional rhabdomyolysis, and malignant hyperthermia. *Anesth Analg* 109: 1065–1069, 2009.
19. Castresana J. Selection of conserved blocks from multiple alignments for their use in phylogenetic analysis. *Mol Biol Evol* 17: 540–552, 2000.
20. Chan J, Whitten AE, Jeffries CM, Bosanac I, Mal TK, Ito J, Porumb H, Michikawa T, Mikoshiba K, Trehwella J, Ikura M. Ligand-induced conformational changes via flexible linkers in the amino-terminal region of the inositol 1,4,5-trisphosphate receptor. *J Mol Biol* 373: 1269–1280, 2007.
21. Chan J, Yamazaki H, Ishiyama N, Seo MD, Mal TK, Michikawa T, Mikoshiba K, Ikura M. Structural studies of inositol 1,4,5-trisphosphate receptor: coupling ligand binding to channel gating. *J Biol Chem* 285: 36092–36099, 2010.
22. Cornelius G, Gebauer G, Techel D. Inositol trisphosphate induces calcium release from *Neurospora crassa* vacuoles. *Biochem Biophys Res Commun* 162: 852–856, 1989.
23. Corrado D, Basso C, Thiene G. Arrhythmogenic right ventricular cardiomyopathy: diagnosis, prognosis, and treatment. *Heart* 83: 588–595, 2000.
24. da Fonseca PC, Morris SA, Nerou EP, Taylor CW, Morris EP. Domain organization of the type 1 inositol 1,4,5-trisphosphate receptor as revealed by single-particle analysis. *Proc Natl Acad Sci USA* 100: 3936–3941, 2003.
25. De Rosa G, Delogu AB, Piastra M, Chiaretti A, Bloise R, Priori SG. Catecholaminergic polymorphic ventricular tachycardia: successful emergency treatment with intravenous propranolol. *Pediatr Emerg Care* 20: 175–177, 2004.
26. De Smedt F, Verjans B, Mailleux P, Erneux C. Cloning and expression of human brain type I inositol 1,4,5-trisphosphate 5-phosphatase. High levels of mRNA in cerebellar Purkinje cells. *FEBS Lett* 347: 69–72, 1994.
27. De Smedt H, Missiaen L, Parys JB, Bootman MD, Mertens L, Van Den Bosch L, Casteels R. Determination of relative amounts of inositol trisphosphate receptor mRNA isoforms by ratio polymerase chain reaction. *J Biol Chem* 269: 21691–21698, 1994.
28. De Smedt H, Missiaen L, Parys JB, Henning RH, Sienaert I, Vanlingen S, Gijssens A, Himpens B, Casteels R. Isoform diversity of the inositol trisphosphate receptor in cell types of mouse origin. *Biochem J* 322: 575–583, 1997.
29. Denborough MA, Forster JF, Lovell RR, Maplestone PA, Villiers JD. Anaesthetic deaths in a family. *Br J Anaesth* 34: 395–396, 1962.
30. Dirksen RT, Avila G. Altered ryanodine receptor function in central core disease: leaky or uncoupled Ca^{2+} release channels? *Trends Cardiovasc Med* 12: 189–197, 2002.
31. Durham WJ, Aracena-Parks P, Long C, Rossi AE, Goonasekera SA, Boncompagni S, Galvan DL, Gilman CP, Baker MR, Shirokova N, Protasi F, Dirksen R, Hamilton SL. RyR1 S-nitrosylation underlies environmental heat stroke and sudden death in Y522S RyR1 knockin mice. *Cell* 133: 53–65, 2008.
32. Eldar M, Pras E, Lahat H. A missense mutation in the CASQ2 gene is associated with autosomal-recessive catecholamine-induced polymorphic ventricular tachycardia. *Trends Cardiovasc Med* 13: 148–151, 2003.
33. Endo M, Tanaka M, Ogawa Y. Calcium induced release of calcium from the sarcoplasmic reticulum of skinned skeletal muscle fibres. *Nature* 228: 34–36, 1970.
34. Fabiato A. Calcium-induced release of calcium from the cardiac sarcoplasmic reticulum. *Am J Physiol Cell Physiol* 245: C1–C14, 1983.
35. Finch E, Turner T, Goldin S. Calcium as a coagonist of inositol 1,4,5-trisphosphate-induced calcium release. *Science* 252: 443–446, 1991.
36. Foskett JK, White C, Cheung KH, Mak DOD. Inositol trisphosphate receptor Ca^{2+} release channels. *Physiol Rev* 87: 593–658, 2007.
37. Furuichi T, Furutama D, Hakamata Y, Nakai J, Takeshima H, Mikoshiba K. Multiple types of ryanodine receptor/ Ca^{2+} release channels are differentially expressed in rabbit brain. *J Neurosci* 14: 4794–4805, 1994.
38. Furuichi T, Yoshikawa S, Miyawaki A, Wada K, Maeda N, Mikoshiba K. Primary structure and functional expression of the inositol 1,4,5-trisphosphate-binding protein P400. *Nature* 342: 32–38, 1989.
39. Giannini G, Clementi E, Ceci R, Marziali G, Sorrentino V. Expression of a ryanodine receptor- Ca^{2+} channel that is regulated by TGF-beta. *Science* 257: 91–94, 1992.
40. Giannini G, Conti A, Mammarella S, Scrobogna M, Sorrentino V. The ryanodine receptor/calcium channel genes are widely and differentially expressed in murine brain and peripheral tissues. *J Cell Biol* 128: 893–904, 1995.
41. Gyorke I, Hester N, Jones LR, Gyorke S. The role of calsequestrin, triadin, and junctin in conferring cardiac ryanodine receptor responsiveness to luminal calcium. *Biophys J* 86: 2121–2128, 2004.
42. Hakamata Y, Nakai J, Takeshima H, Imoto K. Primary structure and distribution of a novel ryanodine receptor/calcium release channel from rabbit brain. *FEBS Lett* 312: 229–235, 1992.
43. Hamada K, Miyata T, Mayanagi K, Hirota J, Mikoshiba K. Two-state conformational changes in inositol 1,4,5-trisphosphate receptor regulated by calcium. *J Biol Chem* 277: 21115–21118, 2002.
44. Hamada K, Terauchi A, Mikoshiba K. Three-dimensional rearrangements within inositol 1,4,5-trisphosphate receptor by calcium. *J Biol Chem* 278: 52881–52889, 2003.
45. Haugaa KH, Leren IS, Berge KE, Bathen J, Loennechen JP, Anfinsen OG, Fruh A, Edvardsen T, Kongsgard E, Leren TP, Amlie JP. High prevalence of exercise-induced arrhythmias in catecholaminergic polymorphic ventricular tachycardia mutation-positive family members diagnosed by cascade genetic screening. *Europace* 12: 417–423, 2010.
46. Hayashi M, Denjoy I, Extramiana F, Maltret A, Buisson NR, Lupoglazoff JM, Klug D, Takatsuki S, Villain E, Kamblock J, Messali A, Guicheney P, Lunardi J, Leenhardt A. Incidence and risk factors of arrhythmic events in catecholaminergic polymorphic ventricular tachycardia. *Circulation* 119: 2426–2434, 2009.
47. Hopkins PM, Ellis FR, Halsall PJ. Evidence for related myopathies in exertional heat stroke and malignant hyperthermia. *Lancet* 338: 1491–1492, 1991.
48. Hwang HS, Hasdemir C, Laver D, Mehra D, Turhan K, Faggioni M, Yin H, Knollmann BC. Inhibition of cardiac Ca^{2+} release channels (RyR2) determines efficacy of class I antiarrhythmic drugs in catecholaminergic polymorphic ventricular tachycardia. *Circ Arrhythm Electrophysiol* 4: 128–135, 2011.
49. Hymel L, Inui M, Fleischer S, Schindler H. Purified ryanodine receptor of skeletal muscle sarcoplasmic reticulum forms Ca^{2+} -activated oligomeric Ca^{2+} channels in planar bilayers. *Proc Natl Acad Sci USA* 85: 441–445, 1988.
50. Imagawa T, Smith JS, Coronado R, Campbell KP. Purified ryanodine receptor from skeletal muscle sarcoplasmic reticulum is the Ca^{2+} -permeable pore of the calcium release channel. *J Biol Chem* 262: 16636–16643, 1987.
51. Iwai M, Michikawa T, Bosanac I, Ikura M, Mikoshiba K. Molecular basis of the isoform-specific ligand-binding affinity of inositol 1,4,5-trisphosphate receptors. *J Biol Chem* 282: 12755–12764, 2007.
52. Iwai M, Tateishi Y, Hattori M, Mizutani A, Nakamura T, Futatsugi A, Inoue T, Furuichi T, Michikawa T, Mikoshiba K. Molecular cloning of mouse type 2 and type 3 inositol 1,4,5-trisphosphate receptors and identification of a novel type 2 receptor splice variant. *J Biol Chem* 280: 10305–10317, 2005.
53. Jiang QX, Thrower EC, Chester DW, Ehrlich BE, Sigworth FJ. Three-dimensional structure of the type 1 inositol 1,4,5-trisphosphate receptor at 2.4 Å resolution. *EMBO J* 21: 3575–3581, 2002.
54. Jungbluth H. Central core disease. *Orphanet J Rare Dis* 2: 25, 2007.
55. Jungbluth H. Multi-minicore Disease. *Orphanet J Rare Dis* 2: 31, 2007.
56. Jungbluth H, Muller CR, Halliger-Keller B, Brockington M, Brown SC, Feng L, Chattopadhyay A, Mercuri E, Manzur AY, Ferreira A, Laing NG, Davis MR, Roper HP, Dubowitz V, Bydder G, Sewry CA, Muntoni F. Autosomal recessive inheritance of RYR1 mutations in a congenital myopathy with cores. *Neurology* 59: 284–287, 2002.
57. Jurkat-Rott K, McCarthy T, Lehmann-Horn F. Genetics and pathogenesis of malignant hyperthermia. *Muscle Nerve* 23: 4–17, 2000.
58. Katoh K, Toh H. Parallelization of the MAFFT multiple sequence alignment program. *Bioinformatics* 26: 1899–1900, 2010.
59. Kobayashi S, Yano M, Suetomi T, Ono M, Tateishi H, Mochizuki M, Xu X, Uchinoumi H, Okuda S, Yamamoto T, Koseki N, Kyushiki H, Ikemoto N, Matsuzaki M. Dantrolene, a therapeutic agent for malignant hyperthermia, markedly improves the function of failing cardiomyocytes by stabilizing interdomain interactions within the ryanodine receptor. *J Am Coll Cardiol* 53: 1993–2005, 2009.
60. Krause T, Gerbershagen MU, Fiege M, Weisshorn R, Wappler F. Dantrolene: a review of its pharmacology, therapeutic use and new developments. *Anaesthesia* 59: 364–373, 2004.
61. Ladenburger EM, Korn I, Kasielke N, Wassmer T, Plattner H. An Ins(1,4,5)P₃ receptor in Paramoecium is associated with the osmoregulatory system. *J Cell Sci* 119: 3705–3717, 2006.
62. Lai FA, Dent M, Wickenden C, Xu L, Kumari G, Misra M, Lee HB, Sar M, Meissner G. Expression of a cardiac Ca^{2+} -release channel isoform in mammalian brain. *Biochem J* 288: 553–564, 1992.
63. Laitinen PJ, Swan H, Kontula K. Molecular genetics of exercise-induced polymorphic ventricular tachycardia: identification of three novel cardiac ryanodine receptor mutations and two common calsequestrin 2 amino-acid polymorphisms. *Eur J Hum Genet* 11: 888–891, 2003.
64. Lanner JT. Ryanodine receptor physiology and its role in disease. *Adv Exp Med Biol* 740: 217–234, 2012.
65. Lanner JT, Georgiou DK, Joshi AD, Hamilton SL. Ryanodine receptors: structure, expression, molecular details, and function in calcium release. *Cold Spring Harb Perspect Biol* 2: a003996, 2010.
66. Lin CC, Baek K, Lu Z. Apo and InsP(3)-bound crystal structures of the ligand-binding domain of an InsP(3) receptor. *Nat Struct Mol Biol* 18: 1172–1174, 2011.
67. Liu N, Ruan Y, Denegri M, Baccetti T, Li Y, Colombi B, Napolitano C, Coetzee WA, Priori SG. Calmodulin kinase II inhibition prevents arrhythmias in RyR2(R4496C+/-) mice with catecholaminergic polymorphic ventricular tachycardia. *J Mol Cell Cardiol* 50: 214–222, 2011.

68. Lobo PA, Kimlicka L, Tung CC, Van Petegem F. The deletion of exon 3 in the cardiac ryanodine receptor is rescued by beta strand switching. *Structure* 19: 790–798, 2011.
69. Lobo PA, Van Petegem F. Crystal structures of the N-terminal domains of cardiac and skeletal muscle ryanodine receptors: insights into disease mutations. *Structure* 17: 1505–1514, 2009.
70. Ludtke SJ, Serysheva II, Hamilton SL, Chiu W. The pore structure of the closed RyR1 channel. *Structure* 13: 1203–1211, 2005.
71. Ludtke SJ, Tran TP, Ngo QT, Moiseenkova-Bell VY, Chiu W, Serysheva II. Flexible architecture of IP3R1 by Cryo-EM. *Structure* 19: 1192–1199, 2011.
72. Mackrill JJ. Ryanodine receptor calcium release channels: an evolutionary perspective. *Adv Exp Med Biol* 740: 159–182, 2012.
73. Maranto AR. Primary structure, ligand binding, and localization of the human type 3 inositol 1,4,5-trisphosphate receptor expressed in intestinal epithelium. *J Biol Chem* 269: 1222–1230, 1994.
74. Marks AR, Priori S, Memmi M, Kontula K, Laitinen PJ. Involvement of the cardiac ryanodine receptor/calcium release channel in catecholaminergic polymorphic ventricular tachycardia. *J Cell Physiol* 190: 1–6, 2002.
75. Marks AR, Tempst P, Hwang KS, Taubman MB, Inui M, Chadwick C, Fleischer S, Nadal-Ginard B. Molecular cloning and characterization of the ryanodine receptor/junctional channel complex cDNA from skeletal muscle sarcoplasmic reticulum. *Proc Natl Acad Sci USA* 86: 8683–8687, 1989.
76. Maryon EB, Coronado R, Anderson P. Unc-68 encodes a ryanodine receptor involved in regulating *C. elegans* body-wall muscle contraction. *J Cell Biol* 134: 885–893, 1996.
77. Masuda W, Takenaka S, Tsuyama S, Tokunaga M, Yamaji R, Inui H, Miyatake K, Nakano Y. Inositol 1,4,5-trisphosphate and cyclic ADP-ribose mobilize Ca^{2+} in a protist, *Euglena gracilis*. *Comp Biochem Physiol C Pharmacol Toxicol Endocrinol* 118: 279–283, 1997.
78. Matsu-ura T, Michikawa T, Inoue T, Miyawaki A, Yoshida M, Mikoshiba K. Cytosolic inositol 1,4,5-trisphosphate dynamics during intracellular calcium oscillations in living cells. *J Cell Biol* 173: 755–765, 2006.
79. Medeiros-Domingo A, Bhuiyan ZA, Tester DJ, Hofman N, Bikker H, van Tintelen JP, Mannens MM, Wilde AA, Ackerman MJ. The RYR2-encoded ryanodine receptor/calcium release channel in patients diagnosed previously with either catecholaminergic polymorphic ventricular tachycardia or genotype negative, exercise-induced long QT syndrome: a comprehensive open reading frame mutational analysis. *J Am Coll Cardiol* 54: 2065–2074, 2009.
80. Meissner G. Ryanodine activation and inhibition of the Ca^{2+} release channel of sarcoplasmic reticulum. *J Biol Chem* 261: 6300–6306, 1986.
81. Mignery GA, Südhof TC, Takei K, De Camilli P. Putative receptor for inositol 1,4,5-trisphosphate similar to ryanodine receptor. *Nature* 342: 192–195, 1989.
82. Moller JV, Olesen C, Winther AM, Nissen P. The sarcoplasmic Ca^{2+} -ATPase: design of a perfect chemi-osmotic pump. *Q Rev Biophys* 43: 501–566, 2010.
83. Muthappan P, Calkins H. Arrhythmogenic right ventricular dysplasia. *Prog Cardiovasc Dis* 51: 31–43, 2008.
84. Nakagawa T, Shiota C, Okano H, Mikoshiba K. Differential localization of alternative spliced transcripts encoding inositol 1,4,5-trisphosphate receptors in mouse cerebellum and hippocampus: in situ hybridization study. *J Neurochem* 57: 1807–1810, 1991.
85. Nakai J, Imagawa T, Hakamat Y, Shigekawa M, Takeshima H, Numa S. Primary structure and functional expression from cDNA of the cardiac ryanodine receptor/calcium release channel. *FEBS Lett* 271: 169–177, 1990.
86. Nakanishi S, Kuwajima G, Mikoshiba K. Immunohistochemical localization of ryanodine receptors in mouse central nervous system. *Neurosci Res* 15: 130–142, 1992.
87. Napolitano C, Priori SG. Diagnosis and treatment of catecholaminergic polymorphic ventricular tachycardia. *Heart Rhythm* 4: 675–678, 2007.
88. Nelson TE. Malignant hyperthermia: a pharmacogenetic disease of Ca^{2+} regulating proteins. *Curr Mol Med* 2: 347–369, 2002.
89. Newton CL, Mignery GA, Südhof TC. Co-expression in vertebrate tissues and cell lines of multiple inositol 1,4,5-trisphosphate (InsP3) receptors with distinct affinities for InsP3. *J Biol Chem* 269: 28613–28619, 1994.
90. Neylon CB, Richards SM, Larsen MA, Agrotis A, Bobik A. Multiple types of ryanodine receptor/ Ca^{2+} release channels are expressed in vascular smooth muscle. *Biochem Biophys Res Commun* 215: 814–821, 1995.
91. Otsu K, Willard HF, Khanna VK, Zorzato F, Green NM, MacLennan DH. Molecular cloning of cDNA encoding the Ca^{2+} release channel (ryanodine receptor) of rabbit cardiac muscle sarcoplasmic reticulum. *J Biol Chem* 265: 13472–13483, 1990.
92. Ottini L, Marziali G, Conti A, Charlesworth A, Sorrentino V. Alpha and beta isoforms of ryanodine receptor from chicken skeletal muscle are the homologues of mammalian RyR1 and RyR3. *Biochem J* 315: 207–216, 1996.
93. Palnitkar SS, Bin B, Jimenez LS, Morimoto H, Williams PG, Paul-Pletzer K, Parness J. [3H]azidodantrolene: synthesis and use in identification of a putative skeletal muscle dantrolene binding site in sarcoplasmic reticulum. *J Med Chem* 42: 1872–1880, 1999.
94. Pamukcoglu T. Sudden death due to malignant hyperthermia. *Am J Forensic Med Pathol* 9: 161–162, 1988.
95. Parness J, Palnitkar SS. Identification of dantrolene binding sites in porcine skeletal muscle sarcoplasmic reticulum. *J Biol Chem* 270: 18465–18472, 1995.
96. Priori SG, Napolitano C, Tiso N, Memmi M, Vignati G, Bloise R, Sorrentino V, Danieli GA. Mutations in the cardiac ryanodine receptor gene (hRyR2) underlie catecholaminergic polymorphic ventricular tachycardia. *Circulation* 103: 196–200, 2001.
97. Prole DL, Taylor CW. Identification of intracellular and plasma membrane calcium channel homologues in pathogenic parasites. *PLoS One* 6: e26218, 2011.
98. Quane KA, Healy JM, Keating KE, Manning BM, Couch FJ, Palmucci LM, Doriguzzi C, Fagerlund TH, Berg K, Ording H, et al. Mutations in the ryanodine receptor gene in central core disease and malignant hyperthermia. *Nat Genet* 5: 51–55, 1993.
99. Radermacher M, Rao V, Grassucci R, Frank J, Timerman AP, Fleischer S, Wagenknecht T. Cryo-electron microscopy and three-dimensional reconstruction of the calcium release channel/ryanodine receptor from skeletal muscle. *J Cell Biol* 127: 411–423, 1994.
100. Robinson R, Carpenter D, Shaw MA, Halsall J, Hopkins P. Mutations in RYR1 in malignant hyperthermia and central core disease. *Hum Mutat* 27: 977–989, 2006.
101. Robinson RL, Brooks C, Brown SL, Ellis FR, Halsall PJ, Quinnell RJ, Shaw MA, Hopkins PM. RYR1 mutations causing central core disease are associated with more severe malignant hyperthermia in vitro contracture test phenotypes. *Hum Mutat* 20: 88–97, 2002.
102. Roderick HL, Berridge MJ, Bootman MD. Calcium-induced calcium release. *Curr Biol* 13: R425, 2003.
103. Rosenberg H, Davis M, James D, Pollock N, Stowell K. Malignant hyperthermia. *Orphanet J Rare Dis* 2: 21, 2007.
104. Ross CA, Danoff SK, Schell MJ, Snyder SH, Ullrich A. Three additional inositol 1,4,5-trisphosphate receptors: molecular cloning and differential localization in brain and peripheral tissues. *Proc Natl Acad Sci USA* 89: 4265–4269, 1992.
105. Rossi AM, Riley AM, Tovey SC, Rahman T, Dellis O, Taylor EJ, Veresov VG, Potter BV, Taylor CW. Synthetic partial agonists reveal key steps in IP3 receptor activation. *Nat Chem Biol* 5: 631–639, 2009.
106. Ryan JF, Tedeschi LG. Sudden unexplained death in a patient with a family history of malignant hyperthermia. *J Clin Anesth* 9: 66–68, 1997.
107. Sakube Y, Ando H, Kagawa H. Cloning and mapping of a ryanodine receptor homolog gene of *Caenorhabditis elegans*. *Ann NY Acad Sci* 707: 540–545, 1993.
108. Samsó M, Feng W, Pessah IN, Allen PD. Coordinated movement of cytoplasmic and transmembrane domains of RyR1 upon gating. *PLoS Biol* 7: e85, 2009.
109. Samsó M, Wagenknecht T, Allen PD. Internal structure and visualization of transmembrane domains of the RyR1 calcium release channel by cryo-EM. *Nat Struct Mol Biol* 12: 539–544, 2005.
110. Sato C, Hamada K, Ogura T, Miyazawa A, Iwasaki K, Hiroaki Y, Tani K, Terauchi A, Fujiyoshi Y, Mikoshiba K. Inositol 1,4,5-trisphosphate receptor contains multiple cavities and L-shaped ligand-binding domains. *J Mol Biol* 336: 155–164, 2004.
111. Seo MD, Velamakanni S, Ishiyama N, Stathopoulos PB, Rossi AM, Khan SA, Dale P, Li C, Ames JB, Ikura M, Taylor CW. Structural and functional conservation of key domains in InsP3 and ryanodine receptors. *Nature* 483: 108–112, 2012.
112. Serysheva II, Bare DJ, Ludtke SJ, Kettlun CS, Chiu W, Mignery GA. Structure of the type 1 inositol 1,4,5-trisphosphate receptor revealed by electron cryomicroscopy. *J Biol Chem* 278: 21319–21322, 2003.
113. Serysheva II, Orlova EV, Chiu W, Sherman MB, Hamilton SL, van Heel M. Electron cryomicroscopy and angular reconstruction used to visualize the skeletal muscle calcium release channel. *Nat Struct Biol* 2: 18–24, 1995.
114. Sewry CA, Muller C, Davis M, Dwyer JS, Dove J, Evans G, Schroder R, Furst D, Helliwell T, Laing N, Quinlivan RC. The spectrum of pathology in central core disease. *Neuromuscul Disord* 12: 930–938, 2002.
115. Sharp AH, McPherson PS, Dawson TM, Aoki C, Campbell KP, Snyder SH. Differential immunohistochemical localization of inositol 1,4,5-trisphosphate- and ryanodine-sensitive Ca^{2+} release channels in rat brain. *J Neurosci* 13: 3051–3063, 1993.
116. Shibao K, Hirata K, Robert ME, Nathanson MH. Loss of inositol 1,4,5-trisphosphate receptors from bile duct epithelia is a common event in cholestasis. *Gastroenterology* 125: 1175–1187, 2003.

117. Shinohara T, Michikawa T, Enomoto M, Goto J, Iwai M, Matsu-ura T, Yamazaki H, Miyamoto A, Suzuki A, Mikoshiba K. Mechanistic basis of bell-shaped dependence of inositol 1,4,5-trisphosphate receptor gating on cytosolic calcium. *Proc Natl Acad Sci USA* 108: 15486–15491, 2011.
118. Südhof TC, Newton CL, Archer BT, Ushkaryov YA, Mignery GA. Structure of a novel InsP₃ receptor. *EMBO J* 10: 3199–3206, 1991.
119. Suetomi T, Yano M, Uchinoumi H, Fukuda M, Hino A, Ono M, Xu X, Tateishi H, Okuda S, Doi M, Kobayashi S, Ikeda Y, Yamamoto T, Ikemoto N, Matsuzaki M. Mutation-linked defective interdomain interactions within ryanodine receptor cause aberrant Ca²⁺ release leading to catecholaminergic polymorphic ventricular tachycardia. *Circulation* 124: 682–694, 2011.
120. Sugawara H, Kurosaki M, Takata M, Kurosaki T. Genetic evidence for involvement of type 1, type 2 and type 3 inositol 1,4,5-trisphosphate receptors in signal transduction through the B-cell antigen receptor. *EMBO J* 16: 3078–3088, 1997.
121. Tae H, Casarotto MG, Dulhunty AF. Ubiquitous SPRY domains and their role in the skeletal type ryanodine receptor. *Eur Biophys J* 39: 51–59, 2009.
122. Takeshima H, Nishimura S, Matsumoto T, Ishida H. Primary structure and expression from complementary DNA of skeletal muscle ryanodine receptor. *Nature* 339: 439–445, 1989.
123. Tamura K, Peterson D, Peterson N, Stecher G, Nei M, Kumar S. MEGA5: molecular evolutionary genetics analysis using maximum likelihood, evolutionary distance, and maximum parsimony methods. *Mol Biol Evol* 28: 2731–2739, 2011.
124. Tamura T, Hashimoto M, Aruga J, Konishi Y, Nakagawa M, Ohbayashi T, Shimada M, Mikoshiba K. Promoter structure and gene expression of the mouse inositol 1,4,5-trisphosphate receptor type 3 gene. *Gene* 275: 169–176, 2001.
125. Tateishi H, Yano M, Mochizuki M, Suetomi T, Ono M, Xu X, Uchinoumi H, Okuda S, Oda T, Kobayashi S, Yamamoto T, Ikeda Y, Ohkusa T, Ikemoto N, Matsuzaki M. Defective domain-domain interactions within the ryanodine receptor as a critical cause of diastolic Ca²⁺ leak in failing hearts. *Cardiovasc Res* 81: 536–545, 2009.
126. Taylor CW, Genazzani AA, Morris SA. Expression of inositol trisphosphate receptors. *Cell Calcium* 26: 237–251, 1999.
127. Taylor CW, Prole DL. Ca²⁺ Signalling by IP₃ Receptors. *Subcell Biochem* 59: 1–34, 2012.
128. Terentyev D, Kubalova Z, Valle G, Nori A, Vedamoorthyrao S, Terentyeva R, Viatchenko-Karpinski S, Bers DM, Williams SC, Volpe P, Gyorko S. Modulation of SR Ca release by luminal Ca and calsequestrin in cardiac myocytes: effects of CASQ2 mutations linked to sudden cardiac death. *Biophys J* 95: 2037–2048, 2008.
129. Tung CC, Lobo PA, Kimlicka L, Van Petegem F. The amino-terminal disease hotspot of ryanodine receptors forms a cytoplasmic vestibule. *Nature* 468: 585–588, 2010.
130. van der Werf C, Kannankeril PJ, Sacher F, Krahn AD, Viskin S, Leenhardt A, Shimizu W, Sumitomo N, Fish FA, Bhuiyan ZA, Willems AR, van der Veen MJ, Watanabe H, Laborde J, Haissaguerre M, Knollmann BC, Wilde AA. Flecainide therapy reduces exercise-induced ventricular arrhythmias in patients with catecholaminergic polymorphic ventricular tachycardia. *J Am Coll Cardiol* 57: 2244–2254, 2011.
131. Vandecaetsbeek I, Vangheluwe P, Raeymaekers L, Wuytack F, Vanoevelen J. The Ca²⁺ pumps of the endoplasmic reticulum and Golgi apparatus. *Cold Spring Harb Perspect Biol* 3: a004184, 2011.
132. Vermassen E, Parys JB, Mauger JP. Subcellular distribution of the inositol 1,4,5-trisphosphate receptors: functional relevance and molecular determinants. *Biol Cell* 96: 3–17, 2004.
133. Vest JA, Wehrens XH, Reiken SR, Lehnart SE, Dobrev D, Chandra P, Danilo P, Ravens U, Rosen MR, Marks AR. Defective cardiac ryanodine receptor regulation during atrial fibrillation. *Circulation* 111: 2025–2032, 2005.
134. Ward A, Chaffman MO, Sorkin Dantrolene EM. A review of its pharmacodynamic and pharmacokinetic properties and therapeutic use in malignant hyperthermia, the neuroleptic malignant syndrome and an update of its use in muscle spasticity. *Drugs* 32: 130–168, 1986.
135. Watanabe H, Chopra N, Laver D, Hwang HS, Davies SS, Roach DE, Duff HJ, Roden DM, Wilde AA, Knollmann BC. Flecainide prevents catecholaminergic polymorphic ventricular tachycardia in mice and humans. *Nat Med* 15: 380–383, 2009.
136. Wehrens XH, Marks AR. Altered function and regulation of cardiac ryanodine receptors in cardiac disease. *Trends Biochem Sci* 28: 671–678, 2003.
137. Wehrens XH, Marks AR. Novel therapeutic approaches for heart failure by normalizing calcium cycling. *Nat Rev Drug Discov* 3: 565–573, 2004.
138. Yamazaki H, Chan J, Ikura M, Michikawa T, Mikoshiba K. Tyr-167/Trp-168 in type 1/3 inositol 1,4,5-trisphosphate receptor mediates functional coupling between ligand binding and channel opening. *J Biol Chem* 285: 36081–36091, 2010.
139. Yoshikawa F, Morita M, Monkawa T, Michikawa T, Furuichi T, Mikoshiba K. Mutational analysis of the ligand binding site of the inositol 1,4,5-trisphosphate receptor. *J Biol Chem* 271: 18277–18284, 1996.
140. Zhang Y, Chen HS, Khanna VK, De Leon S, Phillips MS, Schappert K, Britt BA, Browell AK, MacLennan DH. A mutation in the human ryanodine receptor gene associated with central core disease. *Nat Genet* 5: 46–50, 1993.
141. Zorzato F, Fujii J, Otsu K, Phillips M, Green NM, Lai FA, Meissner G, MacLennan DH. Molecular cloning of cDNA encoding human and rabbit forms of the Ca²⁺ release channel (ryanodine receptor) of skeletal muscle sarcoplasmic reticulum. *J Biol Chem* 265: 2244–2256, 1990.